Experimental Research on Night Heat Loss and Dust Effect of Distillation-Solar Chimney Power Plant

Lu Zuo*, [a], Long Huang [a], Pengzhan Dai [a], Yu Chen [a], Shi Chen [a], Siheng Liu [a], Yunting Ge [b]

[a] College of Energy and Electrical Engineering, Hohai University, Nanjing, China

[b] School of the Built Environment and Architecture, London South Bank University, London, UK

ABSTRACT: To more comprehensively grasp the operating characteristics of the solar chimney power plants combined with distillation and provide a valuable reference for the design and operation of the power plants, a comparative test platform was built in this paper, which adopted manual covering of insulation layer and dust, and explored for the first time the impact of the insulation layer and dust accumulation on the operational characteristics of power plants. The results show that the insulation layer can increase the temperature rise of the airflow at night by a maximum of 2.1 °C, which is 25.9%; but at the same time, it will reduce the temperature difference between the seawater and the solar still cover, resulting in a decrease of more than 7% in daily water yield. Therefore, if the power plant pursues water production, it is not necessary to install insulation layers. Dust accumulation will affect the heat collection and storage performance of the system, reduce the power output, and shorten the effective power generation time; at the same time, lowering the seawater temperature will also reduce the water yield of the system by more than 10%, so the power plant must regularly clean the collector roof.

Keywords: Solar chimney power plant; Desalination; Heat collector; Insulation layer; Dust accumulation effect

1 Introduction

The solar chimney power plant combined with distillation system (SCPPCD)[1] is based on the solar chimney power plant (SCPP). The collector is the greenhouse of

* Corresponding author.

E-mail address: zuoluhhu@163.com (L. Zuo).

SCPP, which raises the temperature of the air inside the collector, and forms a temperature difference with the atmosphere outside the collector to generate thermal pressure, which promotes the buoyancy of the heated air in the collector. Under the action of the chimney effect, the heated air will flow radially to the center of the collector. It then flows strongly into the chimney along the contractive diversion channel and pushes the turbine engine at the base of the chimney to output power.

Studies have shown that the overall dimension of the collector is one of the important parameters to determine the power generation efficiency of the system [2-7]. Generally speaking, a larger diameter of the collector is beneficial for the airflow to absorb more heat due to a longer flow path [5-7], so it can increase the temperature rise of the airflow in the collector, and thus increase the power generation of the turbine engine. But in fact, the area of the collector is limited. The larger the diameter of the collector, the larger the area of the roof in contact with the external ambient air, and the greater the heat lost from the roof to the ambient air. Especially when the roof temperature is lower than the airflow temperature, the heat loss of the airflow is severe, which is very unfavorable to the power generation performance of the system [8, 9]. Li et al. [10] also pointed out that the maximum radius of the collector of the Spanish prototype power plant is 380 m. Within this limit, it is hoped to expand the diameter of the collector. But if the limit is exceeded, the thermal balance between the heat loss of the collector and the heat gain from incident solar radiation will be disrupted, with no apparent benefit to power output. Kalash et al. [11] studied the temperature distribution in the sloped solar collector through an experiment, and the results show that the airflow temperature will be higher than the roof temperature at night, resulting in heat loss. Therefore, some thermal insulation measures are needed. Balijepalli et al. [12] established a mathematical model for the energy loss in the collector and found out that when there is solar radiation, the total energy loss through the roof is 18100.4 W, accounting for 30.6% of the total absorbed energy of the collector.

Ambient crosswind is one of the important environmental parameters affecting the

power generation efficiency of the system. The increase of ambient crosswind speed will not only deteriorate the flow state under the roof and increase the driving force of the wind at the chimney outlet but also increase the convective heat transfer coefficient of the collector roof to the ambient atmosphere, thereby increasing the heat loss from the roof to the environment [13-16], especially at night.

Zuo et al. [17] through the experiment found that: in the period of other than 9:00 -15:00, the temperature of airflow was higher than the roof temperature. In this case, the airflow instead heated the roof and continuously lost its heat to the environment. Especially at night, the environmental temperature dropped quickly. Coupled with the influence of the ambient crosswind, the airflow reversely released heat to the environment through the roof, which caused the heat loss to be aggravated and made the airflow temperature drops seriously, and the power output of the system was seriously affected.

The main part of heat loss in the integrated system at night is the roof. Therefore, it is considered to lay a thermal insulation layer on the roof at night or during the period of weak irradiance. This helps to reduce the convective heat transfer between the roof and the ambient air and increase the thermal resistance, so as to reduce heat loss and improve efficiency. To study the specific impact of this measure, it is necessary to further carry out the test and exploration of mitigating the negative impact of nighttime heat dissipation in the roof.

Dust in the environment is considered to be one of the enemies of all solar installations. After the dust is deposited on the transparent surface of the solar installation, the entry of solar rays into the solar installation is hindered, reducing the solar irradiance reaching the interior of the installation [18-21]. The impact of dust pollution on transparent surfaces is often overlooked or underestimated compared to solar irradiance and wind speed, but it may hinder the use and promotion of solar energy equipment. SCPP is a solar thermal system that uses the greenhouse effect to generate electricity, and it is inevitably affected by dust. In 1984, Haaf [22] investigated the effect

of dust accumulation on the light transmission of different collector roof materials. In 2018, Chaichan et al. [23] constructed a small-scale solar chimney test device and exposed this device to the persistent dust storm climate in spring in Iraq to study the effect of dust accumulation on the roof on system performance. The test results show that dust accumulation reduces the solar irradiation entering the system, resulting in a reduction in system efficiency. Mashonjowa et al. [24] tested the effect of dust accumulation on plastic film transmittance. The plastic greenhouse was placed in the environment for 6 months to accumulate dust naturally. The results showed that dust accumulation reduced the transmitted solar radiation by 14%. Al-Kayiem et al. [25] also pointed out that the dust may combine with the dew on the collector roof to produce mud, further reducing the transmittance of the roof. Sangpradit [26] tested the effects of dust and different cleaning methods on the light transmittance of plastic greenhouse cover, and the results showed that the light transmittance of plastic cover decreased by more than 50% after six months of exposure to natural conditions. Tantau et al. [27] found out that evaporation of rainwater caused dust accumulation on the greenhouse roof, resulting in a 10% reduction in the photosynthetic effective radiation transmittance of polymethyl methacrylate. Geoola et al. [28] built a test greenhouse to study the influence of dew and dust on the light transmittance of different cover materials. The results showed that the light transmittance of polycarbonate structural plates with natural dust accumulation for 18 months would lose 12.8%. The above research results show that the role of dust cannot be ignored. However, the review of the literature shows that compared with solar irradiance, researchers pay little attention to the dust on the collector surface of SCPP.

SCPPCD is a solar thermal utilization device. Like SCPP, it also has a huge transparent collector roof. Energy transfer within the system is related to the available solar irradiance and various environmental and climatic factors. Therefore, the optical properties of the transparent roof directly determine the solar radiation absorbed by the seawater thermal storage layer. In practice, the SCPPCD is exposed to the natural

environment for a long time during operation, and dust accumulation will inevitably occur on the roof. This has an adverse effect on the light transmittance of the roof and is not conducive to the system's operation.

However, researchers pay more attention to the optimization of system structure [29], thus lacking studies on the effects of dust on SCPPCD. The SCPPCD is suitable to be built in northwest China, where brackish water resources are abundant. These areas are in aeolian and sandy environments, so the effect of dust accumulation must be considered.

To explore the influence mechanism of mitigating night heat dissipation and surface dust accumulation, this paper uses the SCPPCD comparison test device platform in literature [17] to design two comparison working conditions respectively for the two test contents, and correspondingly transform the original test device. Specifically, for the first test, the integrated test devices with and without a thermal insulation layer were built, and the comparative test was carried out to analyze the actual operation rule and the effect of insulation measures on the output performance, and the countermeasures were proposed. For the second test, build a clean standard device and a dust accumulation comprehensive device, conduct a comparative test to explore the impact mechanism of the dust accumulation on the operation and output characteristics of the integrated system under the actual meteorological conditions, and proposed countermeasures. Because the time required for natural dust accumulation is too long, artificial dust was used to cover the roof in this test.

2 Mathematical Model

Fig. 1 is a schematic diagram of the structure of SCPPCD, which is mainly composed of four parts: solar chimney, transparent collector roof, disc distillation pool, and turbine generator set. The air under the collector roof absorbs solar radiation, the temperature rises and the density decreases, and flows radially into the base of the chimney, driving the turbine to generate electricity; on the other hand, the seawater in the solar distillation pool under the collector roof absorbs heat and evaporates, and

condenses on the cover of the distillation pool to produce fresh water, and at the same time can play the role of heat storage.

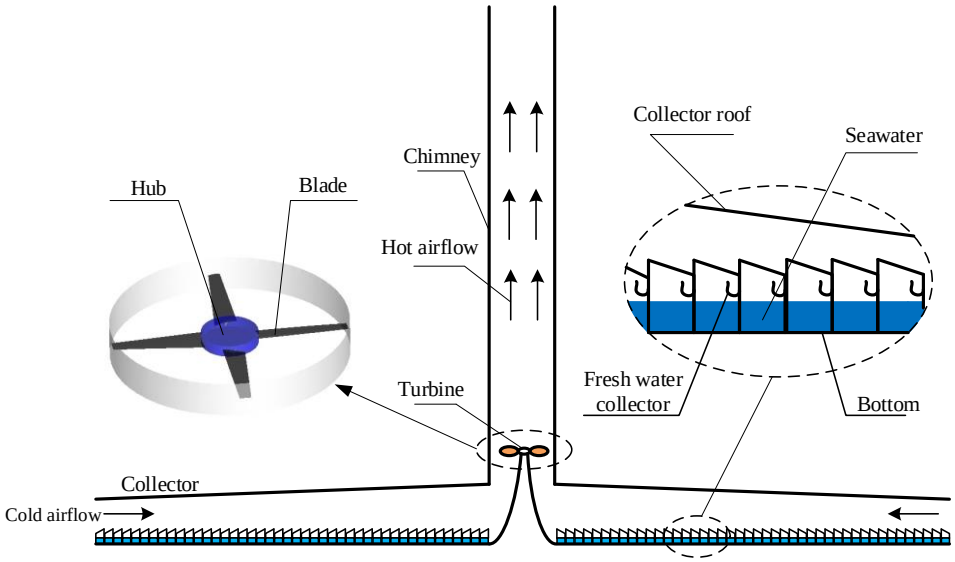

Fig. 1 The structure diagram of the SCPPCD

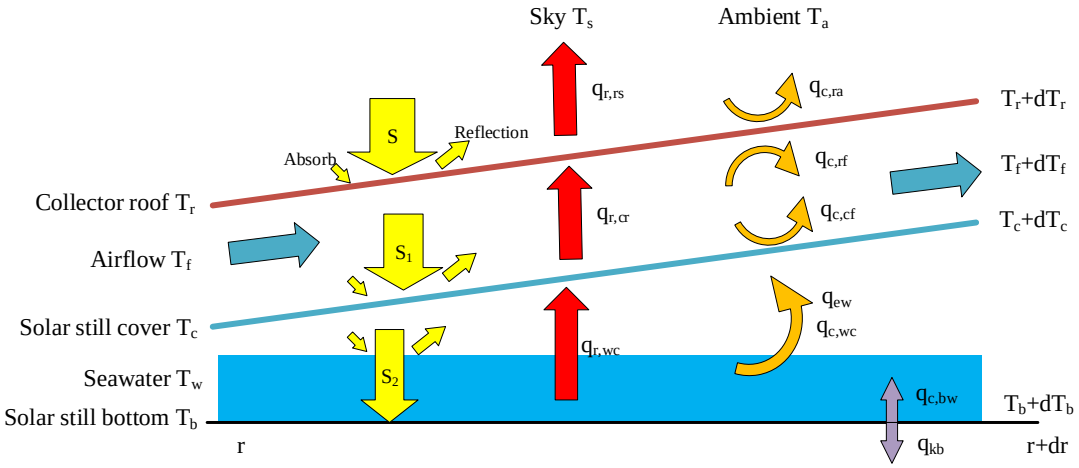

Fig. 2 Control body heat transfer process

Fig. 2 is the energy flow diagram of the system, and the energy balance equation of each component is as follows:

1. The collector roof:

$$\alpha_r S + q_{r,cr} = q_{c,ra} + q_{c,rf} + q_{r,rs} + c_{p,r} M_r \frac{\partial T_r}{\partial t} \tag{1}$$

2. The air in the collector:

$$q_{c,rf} + q_{c,cf} = \frac{C_{p,f} \dot{m}}{s} \frac{\partial T_f}{\partial r} + c_{p,f} \dot{m}_f \frac{\partial T_f}{\partial t} \tag{2}$$

3. The solar still cover:

$$\alpha_c \tau_r S + q_{r,wc} + q_{c,wc} + q_{ew} = q_{r,cr} + q_{c,cf} + c_{p,c} M_c \frac{\partial T_c}{\partial t} \quad (3)$$

4. Seawater layer:

$$\alpha_w \tau_r \tau_c S + q_{c,bw} = q_{r,wc} + q_{ew} + q_{c,wc} + c_{p,w} M_w \frac{\partial T_w}{\partial t} \quad (4)$$

5. Solar still bottom:

$$\alpha_b (1-\alpha_w) \tau_r \tau_c S = q_{c,bw} + q_{kb} + c_{p,b} M_b \frac{\partial T_b}{\partial t} \quad (5)$$

Where α_r is the absorption rate of the collector roof; S is solar irradiance; s is the cavity width, $s = 2\pi r$; τ_r is the light transmittance of the collector roof; For specific calculations for each of the other items, see [30].

3 Experimental setups

Fig. 3 shows the test platform for the test of mitigating night heat dissipation of the roof, and the left one is used as the standard test platform for operation; The one on the right is the comparison test platform with a thermal insulation layer laid on the roof. The insulation layer was added at 18:00 on the test day and removed at 6:00 the next day, that is, the operating time of the system with the insulation layer was 12 hours. The insulation layer used in the test was 10-mm-thick aluminum foil insulation cotton. Under the actual weather conditions, the two comprehensive test devices were tested and compared at the same time, and the test results are preliminarily discussed.

Fig. 4 shows the test platform for the dust accumulation effect. The surface of the roof of the test device on the left was kept clean and it operated as a standard device. The roof surface of the test device on the right was covered with dust for comparison with the standard device. It can be seen from the figure that the dust covers the entire roof, and the distribution is relatively uniform. After the roof is polluted by dust, the obstruction of light will be aggravated, and the solar radiation entering the collector is reduced. Therefore, it is necessary to measure the solar irradiance above and below the roof. In the test, the solar irradiance was measured manually every 30 minutes. The handheld solar radiometer used in the test has a measuring range of 0-2000 W/m^2 and

an accuracy of 0.1 W/m^2.

Fig. 3 Comparative test with and without thermal insulation layer at night

Fig. 4 Comparative test with and without dust accumulation

The structural size of the small-scale SCPPCD test device, distribution of measuring points, and data acquisition system are described in detail in the literature [17], so only a brief introduction of the device is given here with figures.

The structure and dimensions of the test devices are shown in Fig. 5. The device is mainly composed of the roof, ground insulation layer, side walls, solar stills, solar still cover, chimney, and turbine power generator. Among them, the roof adopts a 5 mm thick transparent PC flat sunlight board. The side walls adopt double-layer glass with a 3 mm air gap, and the glass thickness is 3.5 mm. The bottom and wall of the solar stills are made of 8 mm thick plexiglass, the bottom of the solar still is painted black, and the external side and bottom of the stills are paved with 20 mm black rubber plastic insulation material. The solar still cover adopts 3.5 mm thick plate glass. The chimney adopts a grey PVC water pipe. The number of turbine blades is 5, and the diameter is 280 mm, which is made of plastic. There are 6 solar stills in the comprehensive test device. According to the radial direction from the entrance of the collector to the bottom of the chimney, the number of solar stills is 1 to 6 in turn. The water is simulated by sea crystals, each with a depth of 8 cm.

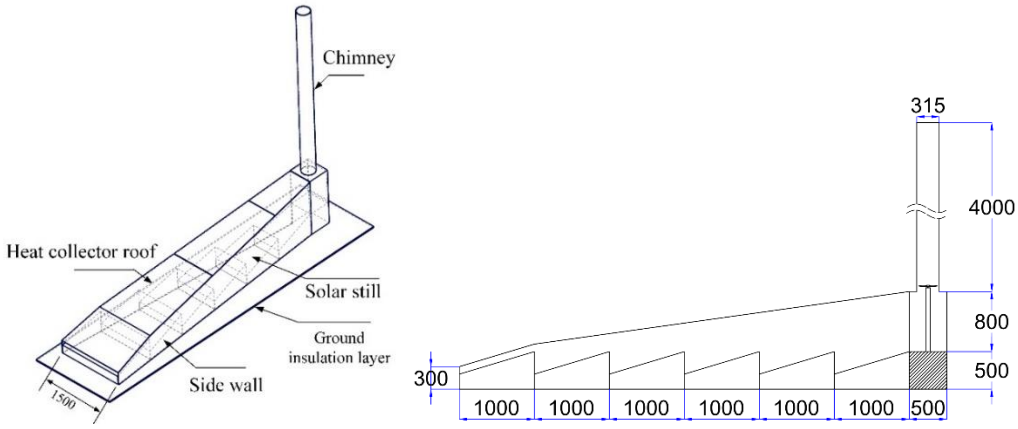

(a) Structural composition of SCPPCD (b) Dimensions of SCPPCD

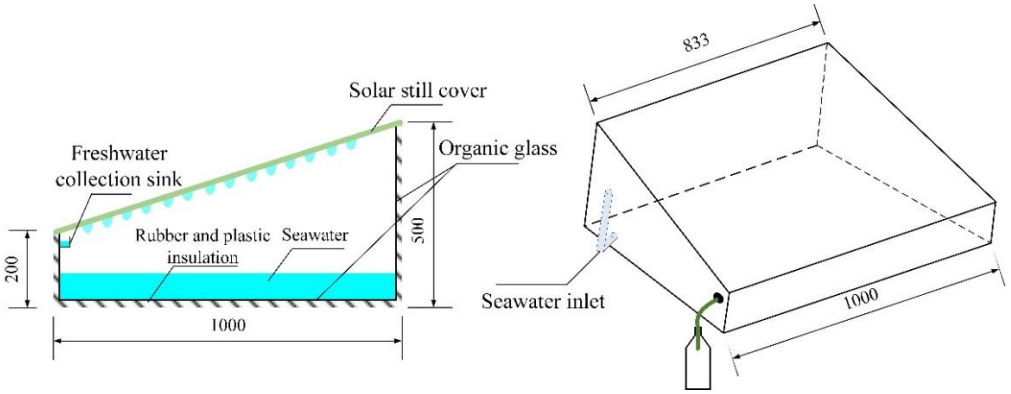

(c) Structure and dimensions of the No. 4 solar still in SCPPCD

Fig. 5 Structure and dimensions of the test devices of SCPPCD (unit: mm)

The data acquisition system and the measuring points are arranged as shown in Fig. 6. The temperature measuring points are numbered 1 to 6 respectively. The interval of automatic data acquisition is 5 minutes. The range and accuracy of the measuring device are shown in Table 1.

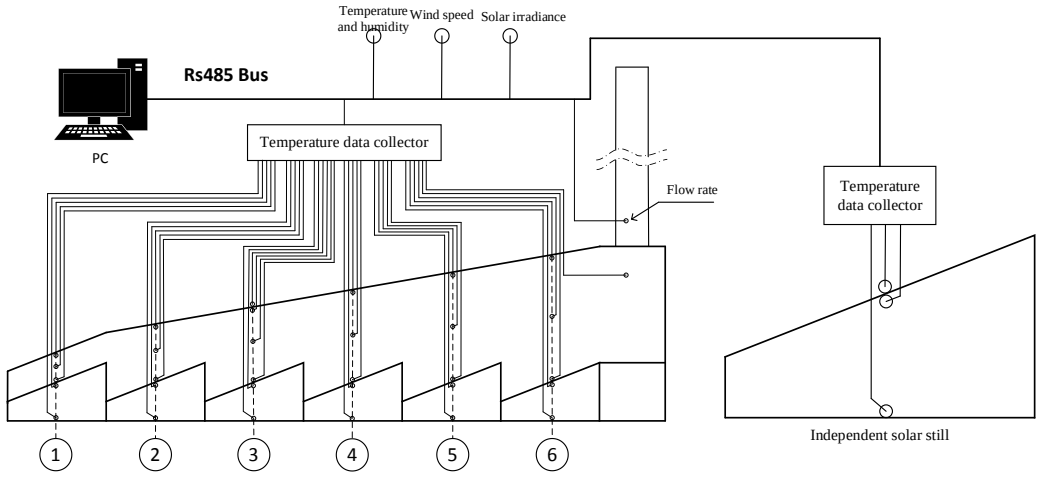

Fig. 6 Measuring point arrangement and the composition of the acquisition system

Table.1 Range and Accuracy of Measurement Devices

Measuring devices	Model	Range	Accuracy
Temperature and humidity sensor	RS-WS-N01-SMG	-40 °C~120 °C 0% RH~80% RH	±0.5 °C, (25 °C) ±3% RH
Three cups wind speed sensor	RS-FSJT-*	0~30 m/s	±(0.2+0.03V) m/s
Pipeline wind speed transmission	RS-FS-*-9TH	0~15 m/s	±(0.2+2%FS) m/s
Temperature Sensor	WZP-PT100	-40 °C~120 °C	±(0.15+0.002T) °C

The uncertainty of measurement parameters is analyzed. The analysis method is introduced in [17]. The results of the analysis are shown in Table 2. The experimental data is sourced from the measured data from 6:00 to 18:00 on August 1, 2021.

Table.2 Uncertainty analysis results of the experimental data

Parameters	Standard error
Ambient temperature	±0.117 ℃
Ambient humidity	±0.461
Airflow and seawater temperature	±0.254 ℃
Ambient wind speed	±0.025 m/s
Airflow velocity in the chimney	±0.028 m/s
Solar irradiance	±14.625 W/m^2

The thermal insulation test date is August 4-7, 2021. The data from August 5 to 6 when the test devices were running stably were discussed. The dust accumulation test date is August 8-11, 2021. The data from August 9 to 10 when the test devices were running stably were discussed.

4 Results and discussion

4.1 Thermal insulation test

4.1.1 Weather conditions

Fig. 7 shows the variation curve of solar irradiance and ambient temperature on the test days. It can be seen from the figure that the two test days are representative of sunny weather in summer.

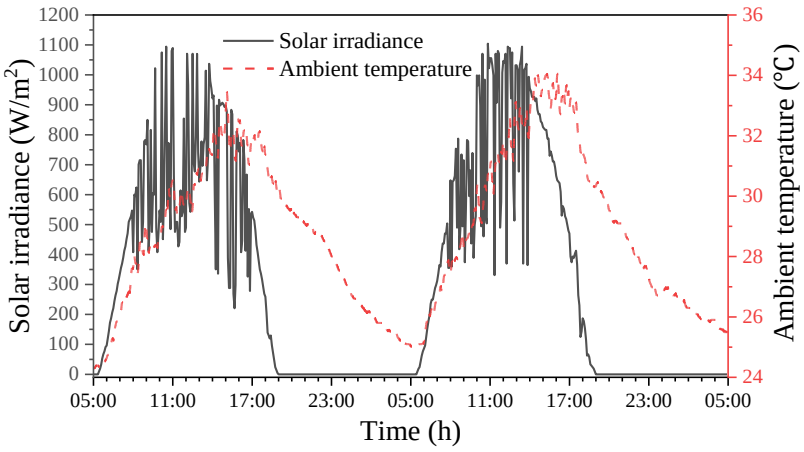

Fig. 7 Variation curves of solar irradiance and ambient temperature on test days

4.1.2 Temperature distribution and variation

Fig. 8 shows the effect of laying the insulation layer at night on the temperature of the roof and airflow. It can be seen from the figure, the temperature of the collector roof continued to rise within an hour after laying the insulation. At 19:00, along the radial direction, the roof temperature was 4.7 °C, 6.6 °C, 6.7 °C, 6.8 °C, 4.8 °C and 4.1 °C higher than the roof temperature in the standard platform. It fell back to the same level as the standard platform within 20 minutes after the insulation was removed at 6:00 the next day. Under the action of the insulation layer, the roof always maintained a higher temperature from 18:00 to 6:00 the next day. In addition, it is found that the temperature increment of the roof first increased and then decreased along the radial direction, and the temperature rise at position 4 was the largest. This was the same as the radial distribution law of the roof temperature.

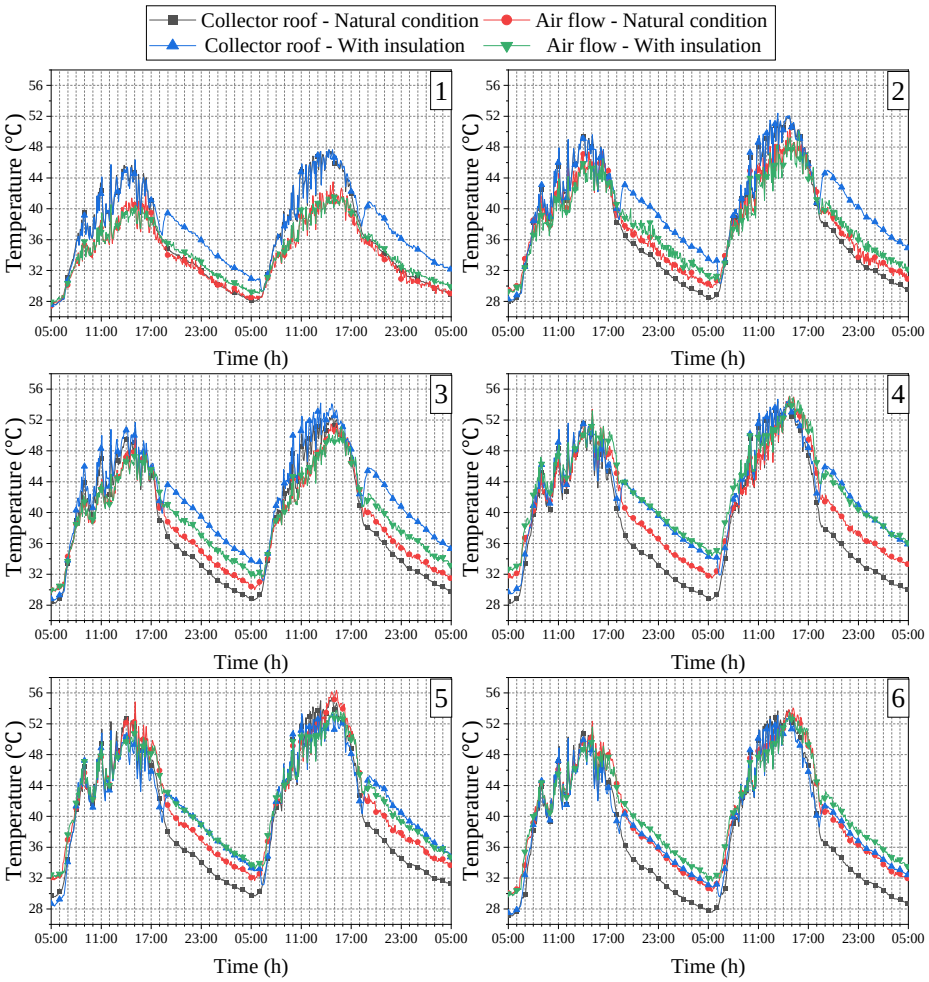

Fig. 8 Comparison of temperature changes in collector roof and hot airflow

It can also be seen from Fig. 8 that during the operation period of the system with an insulation layer, the heat loss phenomenon caused by the airflow reverse heating the roof was improved. After laying the insulation layer, the roof temperature at positions 1, 2, and 3 were higher than the airflow temperature, at positions 4 and 5 were basically the same as the airflow temperature, and only at position 6 was lower than the airflow temperature.

This is because laying the insulation layer greatly reduces the convective and radiative heat dissipation of the roof to the environment and sky, but it will not affect the absorption of radiant heat from the solar still cover. So, the roof temperature rose sharply. At the same time, the airflow temperature also increased slightly, because, in addition to the heating of the seawater, the airflow is also heated by the roof. In the inlet area of the collector, the airflow was greatly affected by the ambient temperature, so the airflow temperature was low, and the positive temperature difference between the roof and the airflow is the largest. In the radial flow process of airflow, with the increase

of seawater temperature, the airflow temperature rise was larger than the roof temperature rise, and the positive temperature difference between them gradually decreased. Their temperatures at positions 4 and 5 were basically the same, and the airflow temperature exceeded the roof temperature at position 6. The test results in Fig. 8 show that the insulation layer has a significant effect on preventing the integrated device from losing heat through the roof at night.

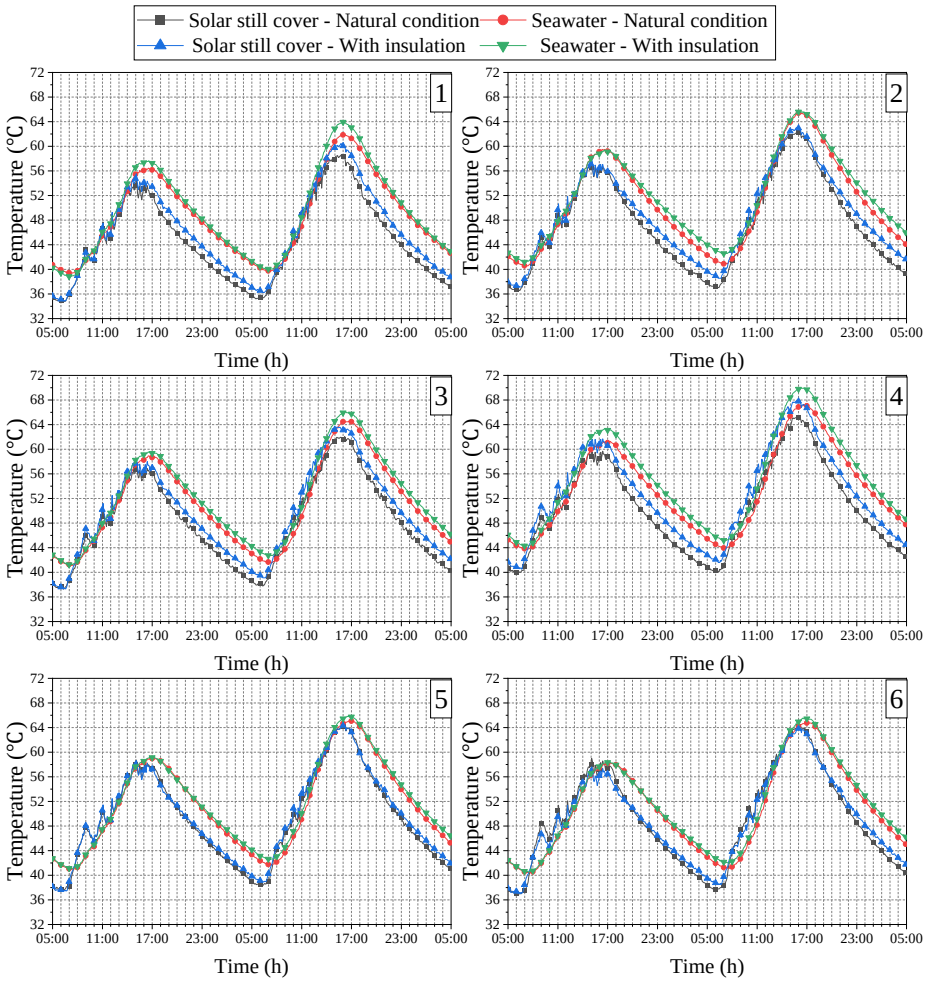

Fig. 9 Comparison of temperature changes in seawater and solar still glass cover

Fig. 9 shows the effect of laying the insulation layer at night on the seawater temperature and the inner surface temperature of the solar still cover. It can be seen from Fig. 9 that the insulation layer has little impact on the seawater temperature and can only slightly increase it. This is because the total heat stored by seawater is high due to its large specific heat capacity, and the heat loss through the roof is small compared with the total heat of seawater. The setting of the insulation layer had a certain impact on the cover temperature. After laying it, the roof temperature rose significantly, and the radiation heat transfer from the cover to the roof is reduced. Relatively, the

cover temperature is higher than that of the natural conditions. However, the increase in the cover temperature is not conducive to the condensation of water vapor.

Fig. 10 shows the effect of laying the insulation layer at night on the temperature difference between seawater and the inner surface of the cover ΔT_{wc}. The temperature difference ΔT_{wc} was reduced during the operating period of the system after setting the insulation layer. During this stage, the average temperature difference of the six temperature measurement points decreased by 1.11 °C, 0.48 °C, 0.59 °C, 0.57 °C, 0.07 °C, and 0.19 °C, respectively. And this period was in the peak water yield period, so the daily water yield decreased.

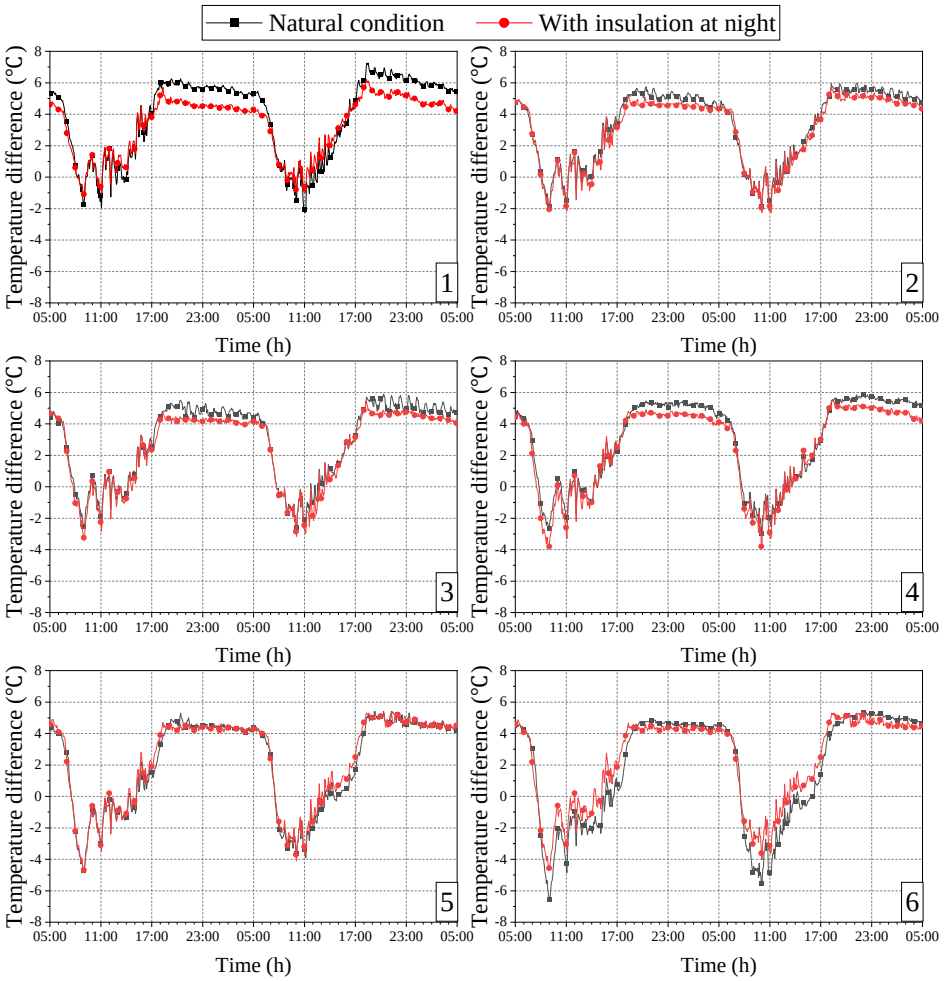

Fig. 10 Comparison of the temperature difference between seawater and solar still cover ΔT_{wc}

4.1.3 Changes in freshwater yield

Fig. 11 shows the comparison of changes in the freshwater yield. After setting the insulation layer at night, the freshwater yield of the six solar stills decreased, especially during the peak water yield period (17:00 to 21:00). The installation of the insulation

layer will reduce the temperature difference between the seawater and the solar still cover, which is not conducive to the condensation of water vapor, thus reducing the water yield of the system, as shown in Table 3.

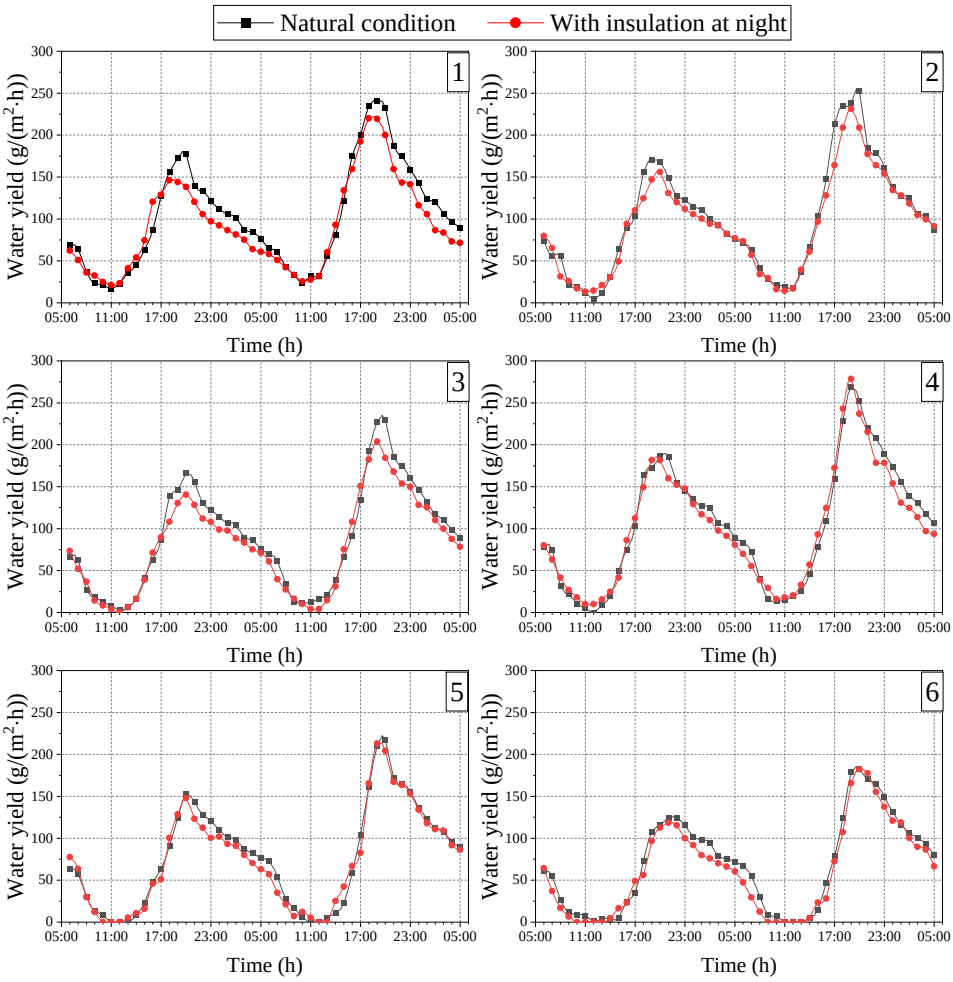

Fig. 11 Comparison of changes in freshwater yield

Table.3 Effect of setting insulation layer at night on daily water yield per unit area

The test day	Daily water yield per unit area (natural conditions) g/(m^2·d)	Daily water yield per unit area (with insulation at night) g/(m^2·d)	Reduced by
2021-8-5	1862.3	1724.0	7.43%
2021-8-6	2490.8	2310.8	7.23%

4.1.4 Power output and solar energy utilization efficiency

The airflow temperature rise at the base of the chimney is an important system operation parameter, which directly affects the output power of the system. Fig. 12 shows the comparison of changes in the airflow temperature rise at the chimney base. After laying the insulation layer at 18:00, there was an obvious sudden rise in airflow

temperature rise. Subsequently, the decreasing speed of the airflow temperature rise under the insulation condition was slower than that under the natural conditions, and the difference in the airflow temperature rise between the two conditions was also gradually increasing. The insulation layer can increase the airflow temperature rise at night by a maximum of 2.1 °C, with an increase of 25.9%. After removing the insulation layer at 6:00 the next day, the airflow temperature rise decreased rapidly until the airflow temperature rise under the two conditions was almost equal. It can be seen that setting the insulation layer can indeed slow down the drop in the airflow temperature rise at night. This is conducive to maintaining the airflow velocity in the chimney and the operation of the turbine and has a positive effect on improving the power generation and smoothing the power output at night. According to the calculation, the increase in the daily average temperature of hot airflow under natural conditions on the 5th and 6th is 9.8 °C and 10.8 °C, respectively. While under insulation conditions, it is 10.3 °C and 11.6 °C, increasing by 5.1% and 7.4%, respectively.

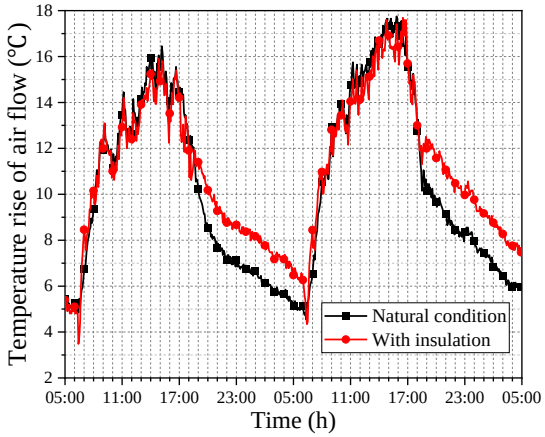

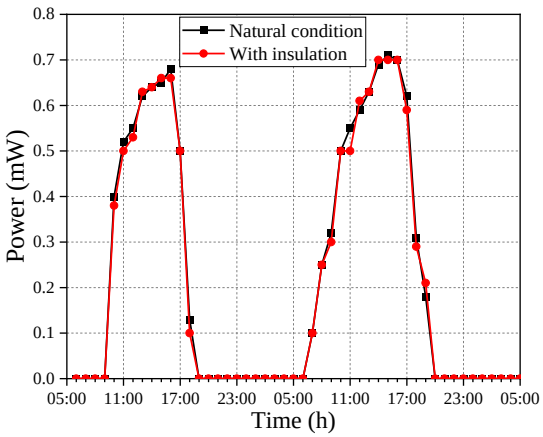

Fig. 12 Comparison of changes in airflow temperature rise Fig. 13 Comparison of changes in generator power

It should be noted that although the setting of the insulation layer slowed down the decline of the airflow temperature rise at night and increased the pressure potential energy and kinetic energy, it was still not enough to drive the turbine to rotate due to the small scale of the test device. So, the output power was 0 W during this period. Therefore, the variation curves of generator power under the two conditions were basically the same, as shown in Fig. 13. From the perspective of the daily utilization

efficiency of solar energy, the average solar energy utilization rate for two days under natural conditions was 18.5%, while it was only 17.1% after using night insulation measures, indicating that laying insulation layers will slightly reduce solar energy utilization efficiency.

4.2 Dust accumulation test

4.2.1 Meteorological conditions

Fig. 14 shows the variation curves of solar irradiance, ambient temperature, and relative humidity on the test days. The figure shows that August 9 can represent a typical sunny day in summer, and August 10 can represent a cloudy day in summer.

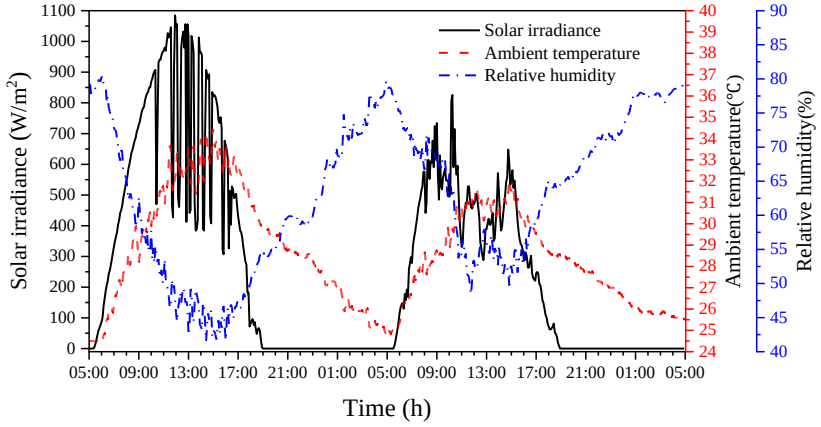

Fig. 14 Variation curves of solar irradiance, ambient temperature, and relative humidity on the test days

4.2.2 Comparison and analysis of solar irradiance above and below the collector roof

Fig. 15 shows the solar irradiance above and below the collector roof under two conditions: keeping the roof clean and covering it with dust. The data in the figure were measured by a hand-held solar radiometer.

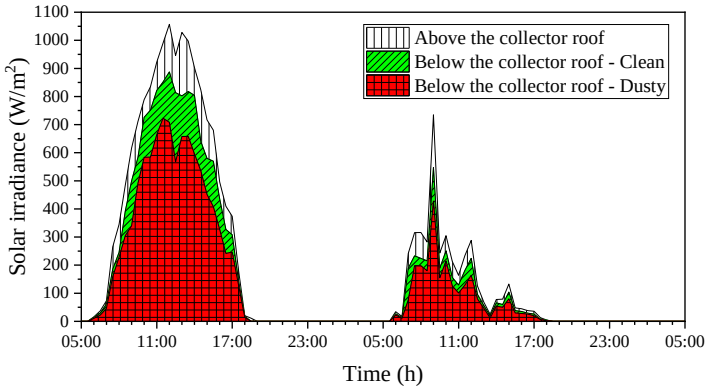

Fig. 15 Solar irradiance above and below the collector roof

As shown in Fig. 15, the roof will absorb a part of the solar radiation whether on a sunny or cloudy day, and reduce the solar radiation transmitted into the system. However, the solar irradiance reduced by the clean roof was much less than that reduced by the dusty roof. The maximum solar irradiance measured manually on August 9 was 1057.0 W/m^2. At this time, the solar irradiance below the clean roof was 887.6 W/m^2, reduced by 16%, and the solar irradiance below the dusty roof was 708.2 W/m^2, reduced by 33%. The maximum solar irradiance on August 10 was 735.0 W/m^2. At this time, the solar irradiance below the clean roof was 547.2 W/m^2, reduced by 25.5%, and the solar irradiance below the dusty roof was 428.1 W/m^2, reduced by 41.7%.

The transmittance of the roof τ_j at the moment j is

$$\tau_j = \frac{I_{b,j}}{I_{a,j}} \tag{6}$$

Where, $I_{a,j}$ represents the solar irradiance above the roof at the moment j, W/m^2. $I_{b,j}$ represents the solar irradiance below the roof at the moment j, W/m^2.

Fig. 16 shows the variation curves of the transmittance of the roof. The transmittance decreased due to the influence of dust accumulation, especially on August 10, indicating that the transmittance performance of the roof deteriorated seriously after it was polluted by dust. By calculation, the average transmittance of the clean roof on August 9 and August 10 was 0.797 and 0.764 respectively, and the average transmittance of the dusty roof was 0.652 and 0.597 respectively. The transmittance was decreased by 0.145 and 0.167 respectively due to dust accumulation, and the weakening of the transmission performance of the roof will inevitably lead to a decrease in the collector efficiency.

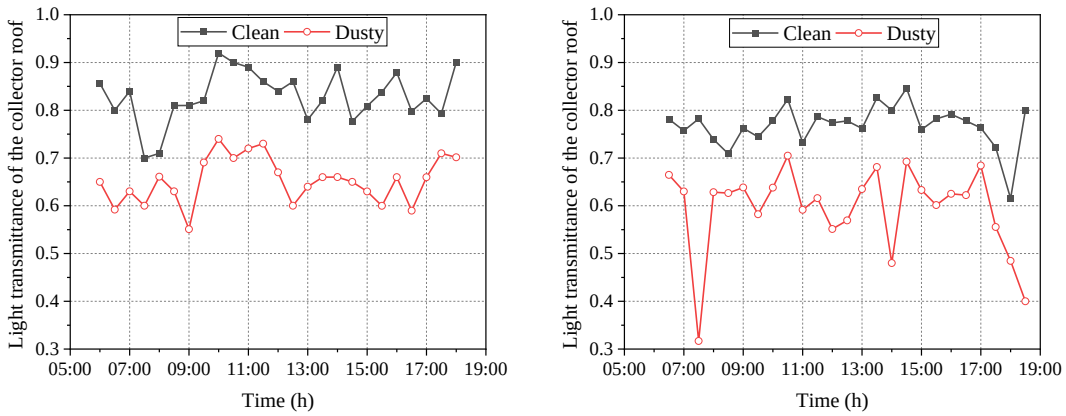

(a) August 9 (b) August 10

Fig. 16 Variation curves of the transmittance of the collector roof

4.2.3 Comparison and analysis of relative temperature on airflow side and generator output power

Fig. 17 shows a comparison of the roof and airflow temperature between the clean device and the dusty device. From Fig. 17, the dust accumulation on the roof has little effect on the roof temperature. Only in the high irradiance time, the dust absorbed more solar radiation energy, so the dusty roof temperature was slightly higher than the clean roof temperature. In other periods, the roof temperature of the two devices was basically equal, and the roof temperature was almost not affected by dust accumulation.

In the area from the collector entrance to the middle part of the collector (that is, positions 1, 2, and 3), the airflow temperature in the two devices had little difference during the all-operation period. In the area from the middle part to the chimney (that is, positions 4, 5, and 6), there was also little difference in the airflow temperature in the two devices between 7:00 and 11:00. But from 11:00 to the next day, the airflow temperature under the dusty roof was lower than that under the clean roof.

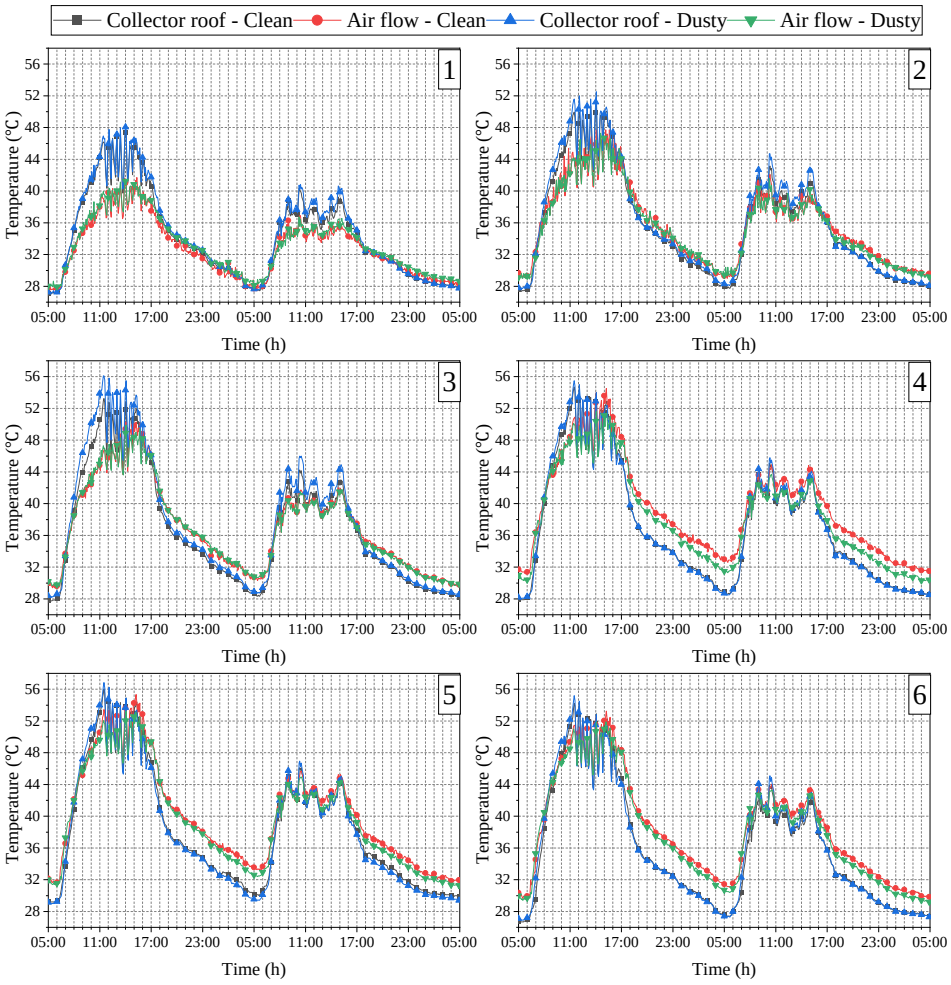

Fig. 17 Variation curves of the temperature of the collector roof and the airflow in the collector

Fig. 18 shows a comparison of the temperature and temperature rise of the airflow in the chimney between the clean device and the dusty device. From Fig. 18(a), the airflow temperature in the chimneys of the two devices was almost the same from 5:00 to 11:00. During this period, dust accumulation on the roof had almost no influence on the airflow temperature in the chimney. After 11:00, the airflow temperature in the chimney of the dusty device dropped and was lower than that of the clean device due to dust accumulation. The effect of dust accumulation lasted until 7:00 on the next day when the airflow temperature of the two test devices was approximately equal again. From 7:00 to 9:00 on the second day, the airflow temperature in the chimneys of the two devices rose almost indifferently. After that, the airflow temperature in the chimney of the dusty device dropped due to the effect of dust accumulation and was lower than that of the clean device, and the decline was even greater than the first day. This is

because the light transmittance of the roof drops too much on the second day, and the system loses more solar radiation energy.

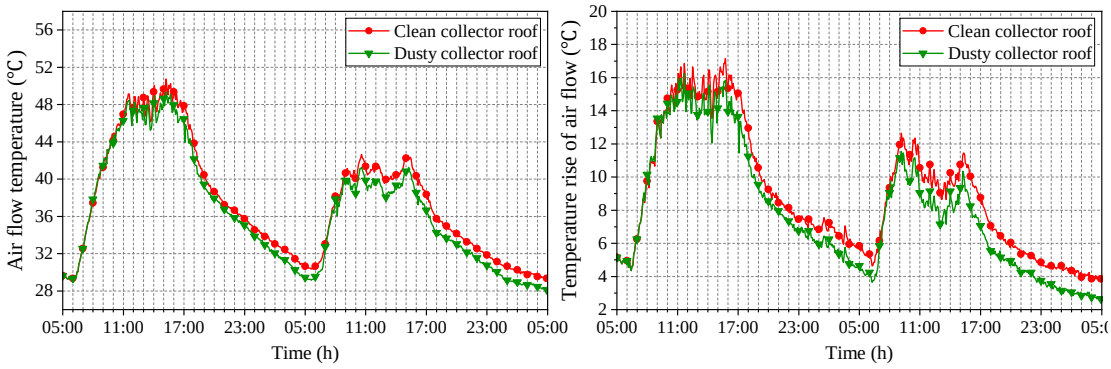

(a) Hot airflow temperature (b)Temperature rise of the hot airflow

Fig. 18 Contrast curves of temperature and temperature rise of the hot air flow in the chimney

Fig. 18(b) shows that the change in the temperature and temperature rise of airflow in the chimney is completely consistent. The effect of dust accumulation on the temperature rise of the airflow in the chimney tended to be obvious from the period of high solar irradiance. It lowered the airflow temperature rise, and the airflow temperature rise dropped more on the second day. From Table 4, it can be seen that dust accumulation will significantly reduce the temperature rise of the airflow and thus reduce power generation.

Table. 4 Effect of dust accumulation on the temperature of hot air flow in the chimney

The test day	Daily mean airflow temperature (°C)			Daily mean airflow temperature rise (°C)		
	Clean device	Dusty device	Reduced by	Clean device	Dusty device	Reduced by
2021-8-9	39.6	38.8	0.8	10.5	9.7	0.8
2021-8-10	35.4	34.2	1.2	7.3	6	1.3

Fig. 19 shows a comparison of the output power of the generator in the clean device and dusty device. Since it was cloudy on August 10, the temperature rise of the airflow in the chimney during the sunshine period was much lower than that on August 9. Therefore, the kinetic energy and pressure potential energy carried by the airflow cannot drive the turbine to rotate, and there was no output power during the sunshine period. Fig. 19 also shows that the output power was decreased significantly during the day and the effective power generation period was shortened due to the effect of dust.

Since there was no power output at night due to the small size of the device, the impact of dust accumulation on the system performance at night cannot be tested. In conclusion, the dust accumulation on the roof greatly affects the power output and is not conducive to the operation of the system.

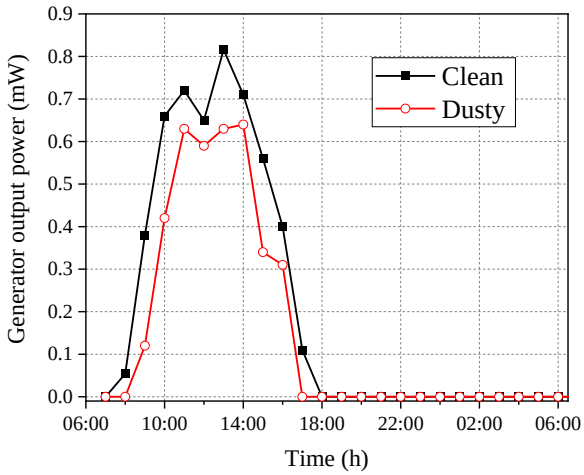

Fig. 19 Comparison of the generator output power

4.2.4 Comparison and analysis of relative temperature on the seawater side and freshwater yield

Fig. 20 shows a comparison of the seawater and solar still cover temperature between the clean device and the dusty device. At sunrise on August 9, the cover temperature in clean and dusty conditions was the same, and so was the seawater temperature. As solar irradiance increased, the seawater and the cover temperature continued to rise, and the two temperatures of the two devices can remain equal for some time. After that, the seawater and cover temperature in the dusty device is gradually lower than that in the clean device. Eventually, except for the No. 1 and No. 3 solar still, the peak temperature of the seawater and cover was reduced due to dust accumulation. And this resulted in the seawater and cover temperature in the dusty device being consistently lower than that in the clean device. The temperature change on August 10 was similar to that on August 9, except for the No. 2 and No. 4 solar still.

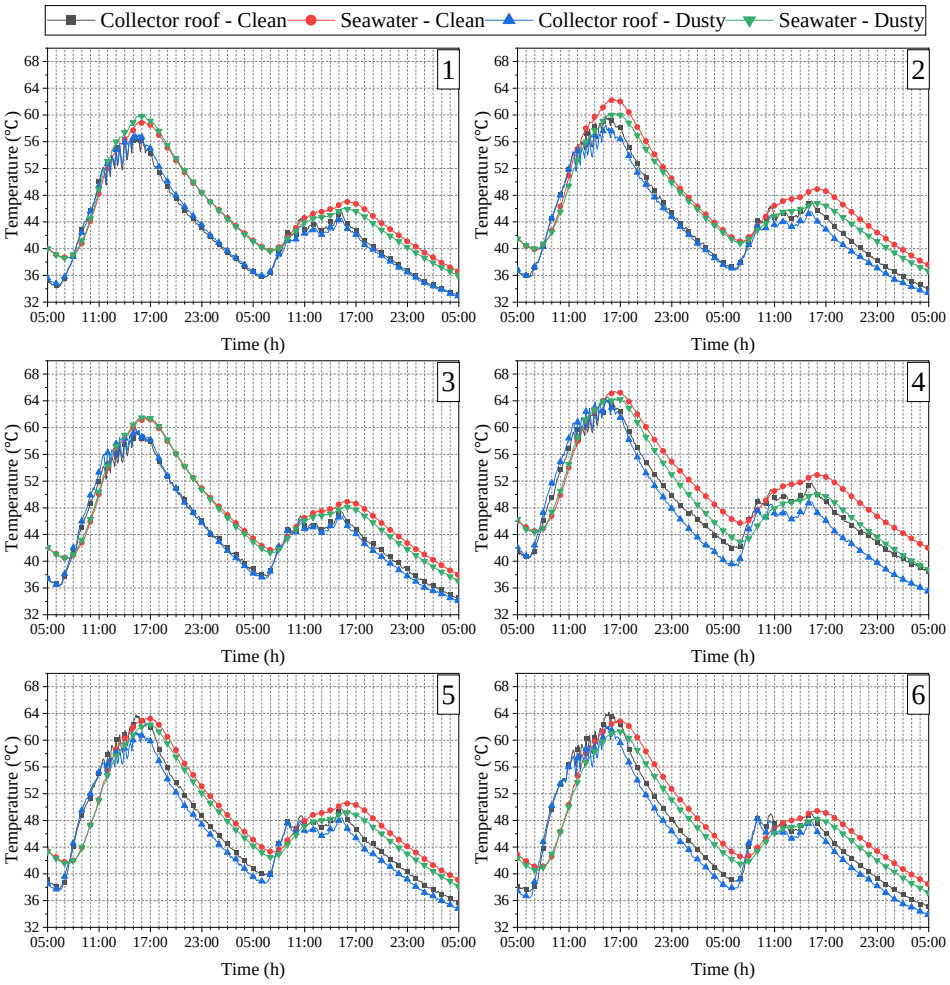

Fig. 20 Contrast curves of seawater temperature and solar still cover temperature

Fig. 21 shows a comparison of the temperature difference between the seawater and the inner surface of the solar still cover ΔT_{cw} between the clean device and the dusty device. It is found that the temperature difference ΔT_{cw} in the two devices is approximately equal, indicating that the influence of dust accumulation on temperature difference ΔT_{cw} is not obvious. From Fig. 20, the dust accumulation reduced both the seawater and cover temperature, so the temperature difference between the two changed very little. According to the analysis in the literature [17]: When the temperature difference is equal, the influence of dust accumulation on the water yield is reflected by seawater temperature. So, the decrease in seawater temperature caused by dust accumulation will directly reduce the freshwater yield.

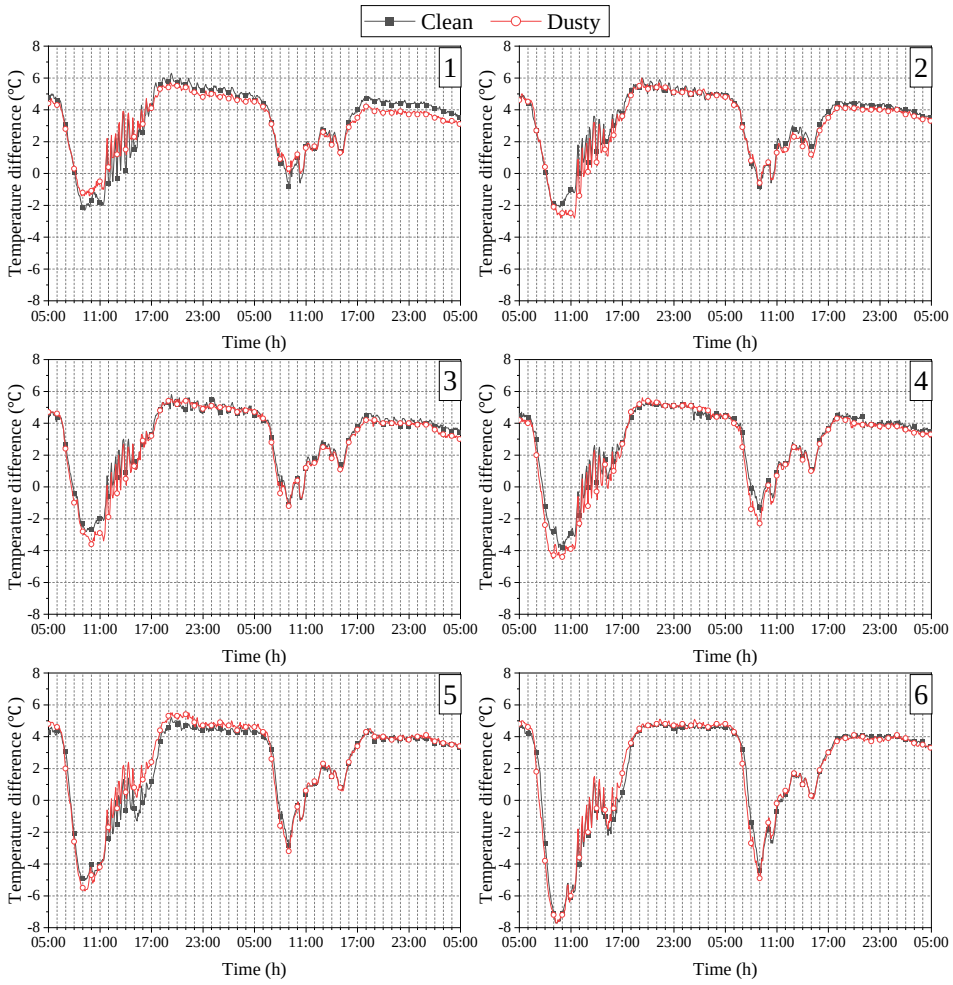

Fig. 21 Comparison of the temperature difference between the seawater and inner surface of solar still cover ΔT_{cw}

Fig. 22 shows a comparison of the water yield between the clean device and the dusty device. Dust accumulation led to a decrease in the hourly water yield per unit area of the six solar stills. On August 9, except for the No. 2 and No. 6 solar still, the water yield in the clean device and dusty device was approximately equal during the rising period of water yield, so the effect of dust accumulation was not obvious. The peak water yield of each solar still in the dusty device was smaller than that in the clean device. On August 10, the water yield of the six solar stills in the dusty device were all smaller than that in the clean device, and the negative effect of dust accumulation was more significant than that on August 9.

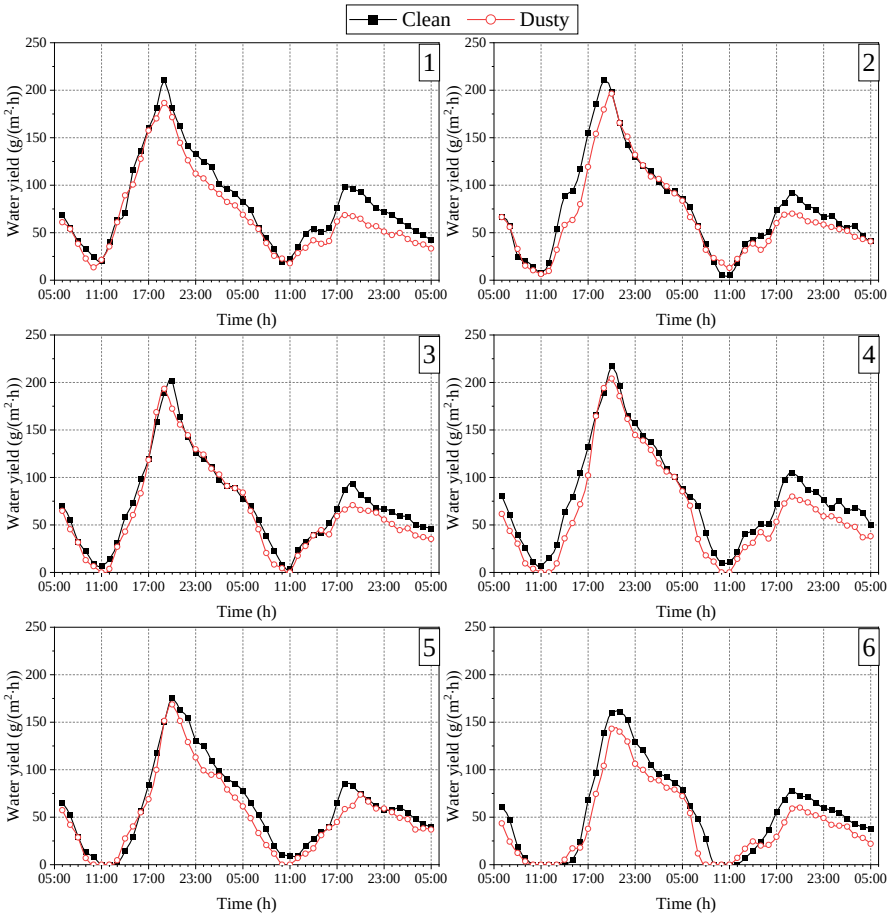

Fig. 22 Comparison of changes in hourly water yield per unit area

Fig. 23 shows a comparison of the radial distribution of the daily water yield in the clean device and dusty device. Table 5 shows the effect of dust accumulation on daily water yield per unit area. It can be seen that the dust accumulation caused a relatively large loss of water yield, and the loss of water yield was greater on August 10.

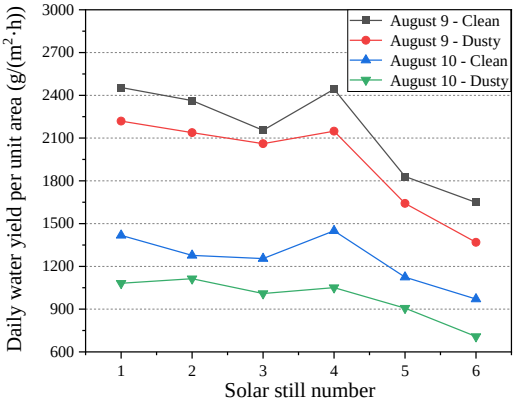

Fig. 23 Comparison of the radial distribution of daily water yield of solar stills

Table.5 Effect of dust accumulation on daily water yield per unit area

The test day	Daily water yield per unit area (clean device) g/(m^2·d)	Daily water yield per unit area (dusty device) g/(m^2·d)	Reduced by
2021-8-9	2149.0	1929.6	10.2%
2021-8-10	1249.0	978.4	21.6%

The test results show that the solar energy utilization rate of the clean cover plate was 17.2%. Dust accumulation reduced the daily utilization efficiency of solar energy, leaving only 14.8%, weakened the system's ability to absorb solar radiation, and reduced the energy conversion efficiency, which is not conducive to the system's operation.

In short, the solar chimney power plant combined with distillation is a multi-objective product output system, and to be effective, the system needs a certain scale. The installation of insulation layers in large-scale integrated systems requires additional installation of relevant devices and mechanisms. Therefore, whether to set up an insulation layer requires balancing the pursued output product goals and technical and economic characteristics. If only from the perspective of energy conversion rate, it is not recommended to install insulation layers in the integrated system. To reduce the impact of dust accumulation, specialized dust removal devices can be set up to regularly remove dust to maintain the cleanliness of the surface of the collector roof. Cuddihy [31] pointed out that outdoor dust accumulation is related to relative humidity and dew. Due to the desalination function of the integrated device, the relative humidity in the area where the system is located may be higher, so it is more important to maintain the cleanliness of the collector roof.

5 Conclusion

In this paper, two kinds of contrast working conditions are designed respectively, and the contrast test bench of the integrated system with and without insulation layer, with and without dust cover were built, the influence mechanism of insulation and dust accumulation on the operation and output characteristics of the integrated system was revealed under the actual meteorological conditions. And propose countermeasures to

improve the operational performance of the system. The results show that:

(1) Adding an insulation layer can significantly improve the heat loss of the collector roof at night, and increase the temperature rise of the hot airflow by a maximum of 2.1 °C, an increase of 25.9%, which is conducive to the smooth operation of the system and the smooth output of electric energy. However, the insulation layer will reduce the temperature difference between the seawater and the solar still cover, which will reduce the daily water production by at least 7%, resulting in a slight decrease in the daily utilization efficiency of solar energy. Whether to set up insulation layers or not depends on the target of output products and technical and economic characteristics.

(2) The dust accumulation on the collector roof will affect the heat collection performance of the collector and the heat storage performance of the distillation pool, resulting in a drop in the seawater temperature and a reduction in freshwater production. Compared with the clean cover, the average daily water yield of the dust cover is reduced by 15.9%. At the same time, the temperature of the airflow is lowered, the power output of the system is reduced, and the effective power generation time is shortened. Therefore, it is necessary for the power plant to regularly clean the collector roof.

Acknowledgment

This research was financially supported by National Natural Science Foundation of China (No. 51976053).

Reference

[1] L. Zuo, Y. Zheng, Z. Li, Y. Sha, Solar chimneys integrated with sea water desalination, Desalination, 276 (2011) 207-213.

[2] J. Pretorius, D. Kröger, Sensitivity Analysis of the Operating and Technical Specifications of a Solar Chimney Power Plant, Journal of Solar Energy Engineering-transactions of The Asme - J SOL ENERGY ENG, 129 (2007).

[3] A. Koonsrisuk, T. Chitsomboon, Effects of flow area changes on the potential of solar chimney power plants, Energy, 51 (2013) 400-406.

[4] A. Arefian, A. Abbassi, R. Hosseini, Exergy analysis and optimisation of collector dimensions in a solar chimney power plant using entropy generation

minimisation method, International Journal of Exergy, 15 (2014) 328-343.
[5] M. Tingzhen, L. Wei, X. Guoliang, Analytical and numerical investigation of the solar chimney power plant systems, International Journal of Energy Research, 30 (2006) 861-873.
[6] K. Milani Shirvan, S. Mirzakhanlari, M. Mamourian, N. Abu-Hamdeh, Numerical investigation and sensitivity analysis of effective parameters to obtain potential maximum power output: A case study on Zanjan prototype solar chimney power plant, Energy Conversion and Management, 136 (2017) 350-360.
[7] A.C. Buğutekin, Effect of the collector diameter on solar chimney power plants, Energy Education Science and Technology Part A: Energy Science and Research, 27 (2011) 155-168.
[8] T. Ming, W. Liu, G. Xu, S.Y. Huang, Y. Pan, Unsteady conjugate numerical simulation of the solar chimney power plant system, Zhongguo Dianji Gongcheng Xuebao/Proceedings of the Chinese Society of Electrical Engineering, 28 (2008) 90-95.
[9] G. Xu, T. Ming, Y. Pan, F. Meng, C. Zhou, Numerical analysis on the performance of solar chimney power plant system, Energy Conversion and Management, 52 (2011) 876-883.
[10] J.-y. Li, P.-h. Guo, Y. Wang, Effects of collector radius and chimney height on power output of a solar chimney power plant with turbines, Renewable Energy, 47 (2012) 21-28.
[11] S. Kalash, W. Naimeh, S. Ajib, Experimental investigation of the solar collector temperature field of a sloped solar updraft power plant prototype, Solar Energy, 98 (2013) 70-77.
[12] R. Balijepalli, V.P. Chandramohan, K. Kirankumar, A complete design data and performance parameter evaluation of a pilot scale solar updraft tower, Heat Transfer Engineering, 41 (2019) 562-575.
[13] X. Zhou, M.A.d.S. Bernardes, R.M. Ochieng, Influence of atmospheric cross flow on solar updraft tower inflow, Energy, 42 (2012) 393-400.
[14] J. Pretorius, D.G. Kröger, The influence of environment on solar chimney power plant performance, R & D Journal of the South African Institution of Mechanical Engineering, 25 (2009) 1-9.
[15] T. Ming, X. Wang, R.K. de Richter, W. Liu, T. Wu, Y. Pan, Numerical analysis on the influence of ambient crosswind on the performance of solar updraft power plant system, Renewable and Sustainable Energy Reviews, 16 (2012) 5567-5583.
[16] W. Shen, T. Ming, Y. Ding, Y. Wu, R.K. de_Richter, Numerical analysis on an industrial-scaled solar updraft power plant system with ambient crosswind, Renewable Energy, 68 (2014) 662-676.
[17] L. Zuo, Z. Yan, P. Dai, T. Zhou, B. Qu, Y. Yuan, Y. Ge, Experimental research on the operation characteristics of solar chimney power plant combined with distillation (SCPPCD), Applied Energy, 326 (2022).
[18] H.A. Kazem, M. Chaichan, Design and Analysis of Standalone Solar Cells in the Desert of Oman, International Journal of Scientific and Engineering Research, 3

(2016) 62-72.
[19] T. Ming, T. Gong, R.K. de Richter, W. Liu, A. Koonsrisuk, Freshwater generation from a solar chimney power plant, Energy Conversion and Management, 113 (2016) 189-200.
[20] H.A. Kazem, M. Chaichan, The Impact of Using Solar Colored Filters to Cover the PV Panel in Its Outcomes, Scholars Bulletin, 2 (2016) 464-469.
[21] H.A. Kazem, M. Chaichan, A. Al-Waeli, K. Mani, Effect of Shadows on the Performance of Solar Photovoltaic, in, 2017, pp. 379-385.
[22] W. Haaf, SOLAR CHIMNEYS - PART II: PRELIMINARY TEST RESULTS FROM THE MANZANARES PILOT PLANT, International Journal of Solar Energy, 2 (1984) 141-161.
[23] M. Chaichan, K. Abass, H.A. Kazem, Dust and Pollution Deposition Impact on a Solar Chimney Performance, International Research Journal of Advanced Engineering and Science, 3 (2018) 127-132.
[24] E. Mashonjowa, F. Ronsse, T. Mhizha, J.R. Milford, R. Lemeur, J.G. Pieters, The effects of whitening and dust accumulation on the microclimate and canopy behaviour of rose plants (Rosa hybrida) in a greenhouse in Zimbabwe, Solar Energy, 84 (2010) 10-23.
[25] H.H. Al-Kayiem, M.A. Aurybi, S.I.U. Gilani, Influence of canopy condensate film on the performance of solar chimney power plant, Renewable Energy, 136 (2019) 1012-1021.
[26] K. Sangpradit, Study of the Solar Transmissivity of Plastic Cladding Materials and Influence of Dust and Dirt on Greenhouse Cultivations, Energy Procedia, 56 (2014) 566-573.
[27] H.J. Tantau, J. Hinken, B. von Elsner, J.F.J. Max, A. Ulbrich, U. Schurr, T. Hofmann, G. Reisinger, Solar Transmittance of Greenhouse Covering Materials, Acta Horticulturae, (2012) 441-448.
[28] F. Geoola, Y. Kashti, U.M. Peiper, A Model Greenhouse for Testing the Role of Condensation, Dust and Dirt on the Solar Radiation Transmissivity of Greenhouse Cladding Materials, Journal of Agricultural Engineering Research, 71 (1998) 339-346.
[29] M. Asayesh, A. Kasaeian, A. Ataei, Optimization of a combined solar chimney for desalination and power generation, Energy Conversion and Management, 150 (2017) 72-80.
[30] L. Zuo, L. Huang, P. Dai, Y. Chen, S. Chen, Y. Ge, Study on refined mathematical model of solar chimney power plant integrated with seawater desalination and the influence of dewing, Desalination, 554 (2023).
[31] E.F. Cuddihy, Theoretical considerations of soil retention, Solar Energy Materials, 3 (1980) 21-33.